融合して用いるアイデアに基づく FUSE を開発した〔4, 5〕. FUSE では，同一患者の SPECT 画像と MRI 画像を用い，脳の萎縮を伴わずに血流が低下している部位を表す DSI 画像（Deterioration Score Image）を出力する．また，SPECT 画像の生成に同一患者の MRI 情報を巧妙に利用して，部分容積効果や統計雑音の影響を軽減して病変を検出しやすい画像を生成する新しい統計的画像再構成法を開発し，FUSE の性能を向上させることに成功した〔6〕．本論文では，これらの研究についてページ数が許す範囲で紹介する．

2. FUSE による脳血流画像解析〔4, 5〕

FUSE は，同一患者の SPECT 画像と MRI 画像を融合して用い，脳の萎縮が伴わずに血流が低下している認知症の目印となる部位を検出する画像解析手法である．FUSE における画像解析は，大きく以下の 3 つのステップから構成される．

1）テンプレート画像の作成：MRI 画像を解析して，正常人の SPECT 画像を模擬したテンプレート画像を作成する．

2）位置合わせ：テンプレート画像と SPECT 画像の位置合わせを行う．

3）DSI 画像の作成と表示：テンプレート画像と SPECT 画像の差分をとり血流低下量の分布を表す DSI 画像を作成し，医師にわかりやすい形で表示する．

以下では，各ステップにおける画像処理について述べる．

1）テンプレート画像の作成

テンプレート画像の作成は，MRI 画像に（1）脳の外側の構造物（骨と皮膚領域）の除去，（2）領域分割，（3）小脳領域の同定，などの画像処理を施した後，次式により行う．

$$f_{temp}(x,y,z) = h_\sigma(x,y,z) * [m_W I_W(x,y,z) + m_G I_G(x,y,z) + m_S I_S(x,y,z)] \quad (1)$$

ただし，* は畳み込み積分を表し，式 (1) における記号の定義を **Table 1** に示す．ガウシアンフィルタで平滑化を行う理由は，テンプレート画像の解像度を SPECT 画像の解像度に一致させるためである．Indicator function(I_W, I_G, I_S) は MRI 画像の領域分割結果から得られる．また，4 つの未知パラメータ (m_W, m_G, m_S, σ) は，テンプレート画像と SPECT 画像の濃度ヒストグラムが一致するように，ヒストグラムマッチング（HM）法と呼ばれる新手法により症例ごとに自動推定する．HM 法では，次式のテンプレート画像と SPECT 画像の濃度ヒストグラム $h_{temp}(i)$, $h_{sp}(i)$ 間の相互相関係数が最大となるように，未知パラメータを推定する．

Table 1 Symbols used to define the template image.

m_W	大脳白質の血流値
m_G	大脳灰質の血流値
m_S	小脳の平均血流値
I_W	大脳白質領域の indicator function
I_G	大脳灰質領域の indicator function
I_S	小脳領域の indicator function
h_σ	半値幅 2.355σ のガウシアンフィルタ

$$C(m_W, m_G, m_S, \sigma) = \sum_i \frac{(h_{temp}(i) - \bar{h}_{temp})(h_{sp}(i) - \bar{h}_{sp})}{\sigma_{temp}\sigma_{sp}} \quad (2)$$

ただし，$\bar{h}_{temp}$, $\bar{h}_{sp}$ は各ヒストグラムの平均を σ_{temp}, σ_{sp} は標準偏差を表す．これにより，撮像装置や撮影条件が違う画像や個人差にもある程度対応できる．なお，このパラメータ推定の際に，SPECT 画像と MRI 画像が位置合わせされている必要はない．最後に，大脳全体の血流値が小脳（基準部位）の血流値より低下している場合を考慮して，大脳の血流値を小脳の血流値で正規化してその影響を補正する．補正後のテンプレート画像は

$$f_{temp-C}(x,y,z) = h_\sigma(x,y,z) * [\frac{m_S}{m_L} m_W I_W(x,y,z) + \frac{m_S}{m_L} m_G I_G(x,y,z) + m_S I_S(x,y,z)] \quad (3)$$

のように表される．ただし，m_L, m_S はおのおの大脳と小脳の平均血流値を表す．

2）位置合わせ

位置合わせは，SPECT 画像 $f_{sp}(x,y,z)$ とテンプレート画像 $f_{temp}(x,y,z)$ の相互相関が最大となるように並進と回転のパラメータを推定し，SPECT 画像をテンプレート画像の座標系へ剛体変換することにより行う．

3）DSI 画像の作成と表示

各ボクセルにおける血流低下量を表す DSI 画像 $DSI(x,y,z)$ を，テンプレート画像 $f_{temp-C}(x,y,$

z) と位置合わせ後の SPECT 画像 $f_{sp}(x,y,z)$ の差分をとり次式で算出する.

$$DSI(x,y,z)=[f_{temp-C}(x,y,z)-f_{sp}(x,y,z)]\frac{m_L}{m_S m_G} \quad (4)$$

そして，医師が視覚的にわかりやすくかつ血流低下部位の MRI 画像上での解剖学的位置が把握できるように，DSI 画像を表示する．具体的には，スライスごとの DSI 画像の表示に加えて，MRI 画像との合成表示（血流低下が一定値以上の画素を MRI 画像上に擬似カラー表示)・表面投影表示（脳表から一定深さ範囲の血流低下量の最大値を脳表に投影して上下前後左右からレンダリング)，の 2 つの表示法を用いる．

FUSE には，統計学的画像解析法と比較して，(1) 正常人画像のデータベースを必要としないこと，(2) (同一患者の SPECT 画像と MRI 画像を比較するため) 脳形状個人差の影響を受けにくいこと，(3) 脳萎縮の影響を排除して純粋な血流異常のみを評価できること，などこの分野におけるブレークスルーと考えられる特徴がある．そこで，3D-SSP と FUSE の比較を含む評価実験を行った．認知症と診断された 9 人の患者に 16 人の正常人を加えた，**Table 2** に内訳を示す 25 症例からなるデータセットを用いた．このデータセットは 3 種類のクラスの画像を含み，クラス認知症 A とクラス認知症 B ＋正常人を判別しやすい結果を出力することが目的となる．SPECT 画像・MRI 画像ともに筑波大学病院で撮影されたものであり，使用した MRI 画像は 2 チャンネル T_1, T_2 である．

Fig. 1 にアルツハイマー病と DLB の症例に対する FUSE の処理結果を示す (文献〔4, 5〕にも他の症例の処理結果がある)．アルツハイマー病の症例では頭頂葉と後部帯状回の血流低下が検出され，DLB の症例では後部全体に広がる大きな血流低下が検出されている．また，3D-SSP と FUSE の両手法により 25 症例のすべてを処理し出力画像を視覚的に比較した結果，クラス認知症 A かクラス認知症 B ＋正常人かの判別は 3D-SSP の Z スコア画像より FUSE の DSI 画像を用いた方が幾分やりやすい傾向が見られた．この事実を客観的に示すため，3D-SSP の Z スコア画像と FUSE の DSI 画像の灰質スコアの平均値 *Zave*, *DSIave* を算出し相関グラフに描いた．その結果を **Fig. 2** に示す．3D-SSP と FUSE の処理結果の間には強い相関が見られ，(症例数は少ないが) FUSE の方が幾分クラス認知症 A とクラス認知症 B ＋正常人を判別しやすい結果を出力していることがわかる．

Table 2 Classification of images contained in the data set.

クラス	SPECT 画像	数
認知症 A	脳の萎縮を伴わずに血流が低下している部位が存在	7
認知症 B	脳の萎縮を伴わずに血流が低下している部位がない	2
正常人	脳の萎縮も血流の低下もない	16

3. MRI 情報を用いた画像再構成〔6〕

近年の SPECT／PET 装置は統計雑音の抑制効果が大きい最尤推定に基づく統計的画像再構成法を採用しているものが多いが，画質改善の効果には限界がある．そこで，同一患者の MRI 画像を用いて，血流低下部位を検出しやすく SPECT 画像を再構成する新しい統計的画像再構成法（Anatomic-MAP 法と呼ぶ）を開発した．

始めに，定性的に Anatomic-MAP 法の考え方を述べる．SPECT で対象とする画像 $f(x,y)$ は，**Fig. 3** に示すように同一組織内で滑らかに変化する背景画像 $f_b(x,y)$ に小さな病変部を表すスポット画像 $f_s(x,y)$ を加えた次式の SOS（Spots on Smooth）モデルで表すことができる．

$$f(x,y)=f_b(x,y)+f_s(x,y) \quad (5)$$

たとえば，このモデルで表すことができる疾患の種類として，認知症の他にがん・てんかん・心筋梗塞などがあげられる．Anatomic-MAP 法は，同一患者の MRI 画像を用いて，SOS モデルで表される画像の小さな病変部に相当するスポットを，(スポットを高コントラストで保存したまま背景の雑音を抑制して) 検出しやすく再構成することを目的とした画像再構成法である．まず，同一患者の MRI 画像に画像処理を施して，背景画像 $f_b(x,y)$ (テンプレート画像と呼ぶ) を推定する．そして，統計的画像再構成の評価関数に背景画像と再構成画像の距離を加えて再構成を行う．これにより背景画像との差が小さくなるように再構成され，距離の選び方によっては平坦部の統計雑音抑制とスポットのコントラスト

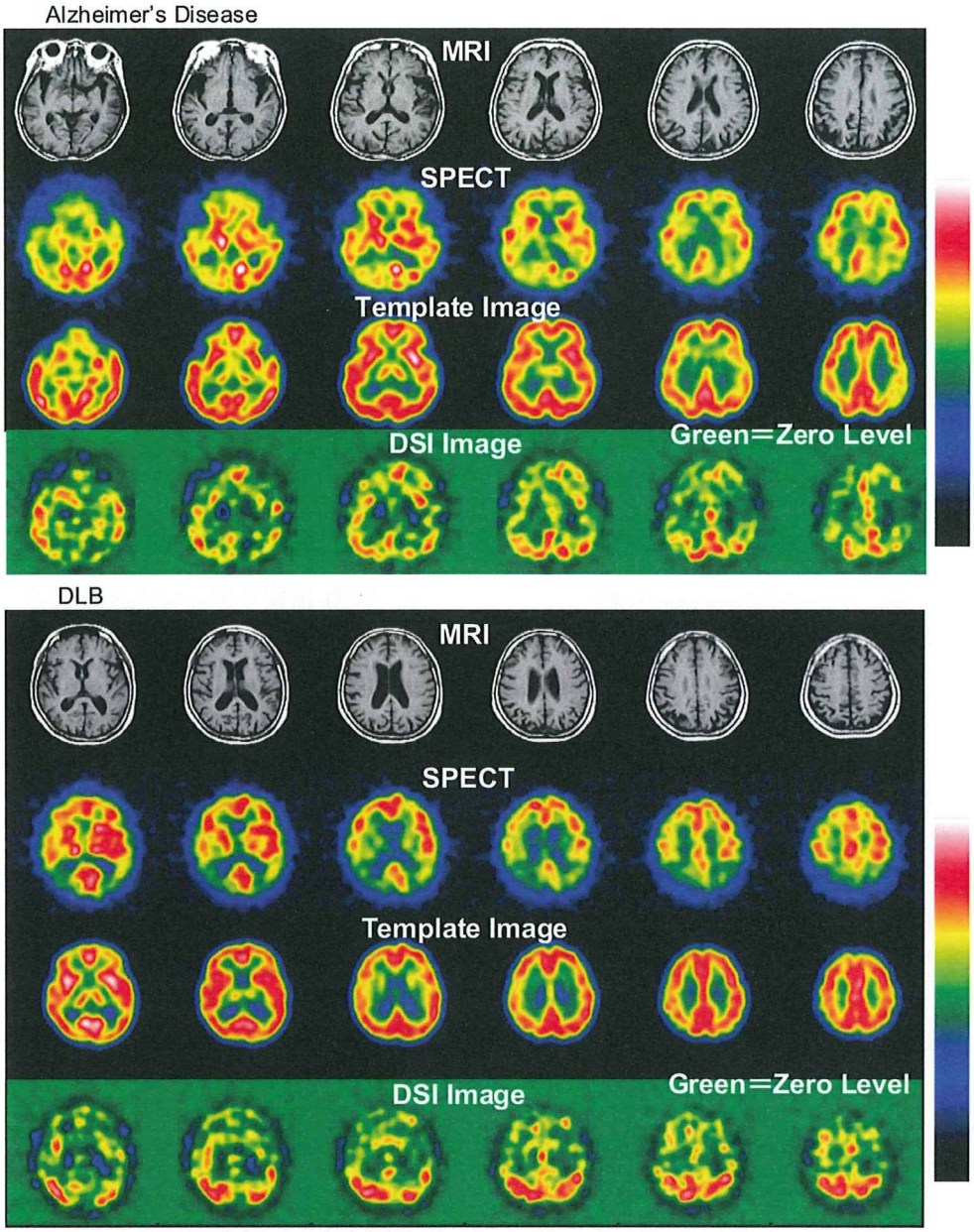

Fig. 1 Two examples of the processed results by FUSE. Other examples can be found in Refs.[4,5].

保存を両立した病変を検出しやすい画像を生成することが可能となる．以下では，脳血流画像への適用を例として，MRI 画像からテンプレート画像を作成する手順と Anatomic-MAP 法の画像再構成について述べる．

1）テンプレート画像の作成

テンプレート画像 $f_b(x,y)$ の作成には FUSE と同じ画像処理手法を用いるが，同一領域の血流値を一定とみなす近似が十分でない場合に対応するため，各領域の濃度変化を低次の多項式で表す Facet モデルを採用している．

2）Anatomic-MAP 画像再構成

まず，統計的手法による SPECT 画像再構成の定式化を行う．対象画像を n 次元ベクトル $\mathbf{x}=(x_1, x_2,\cdots,x_n)$，投影データを m 次元ベクトル $\mathbf{b}=(b_1, b_2,\cdots,b_m)$ で表す．また，投影演算を $m\times n$ 行列 $A=\{a_{ij}\}$ で表す．統計的画像再構成では，MAP 推定に基づいて構成される以下の評価関数 $f(\mathbf{x})$ を最小化することにより再構成を行う．

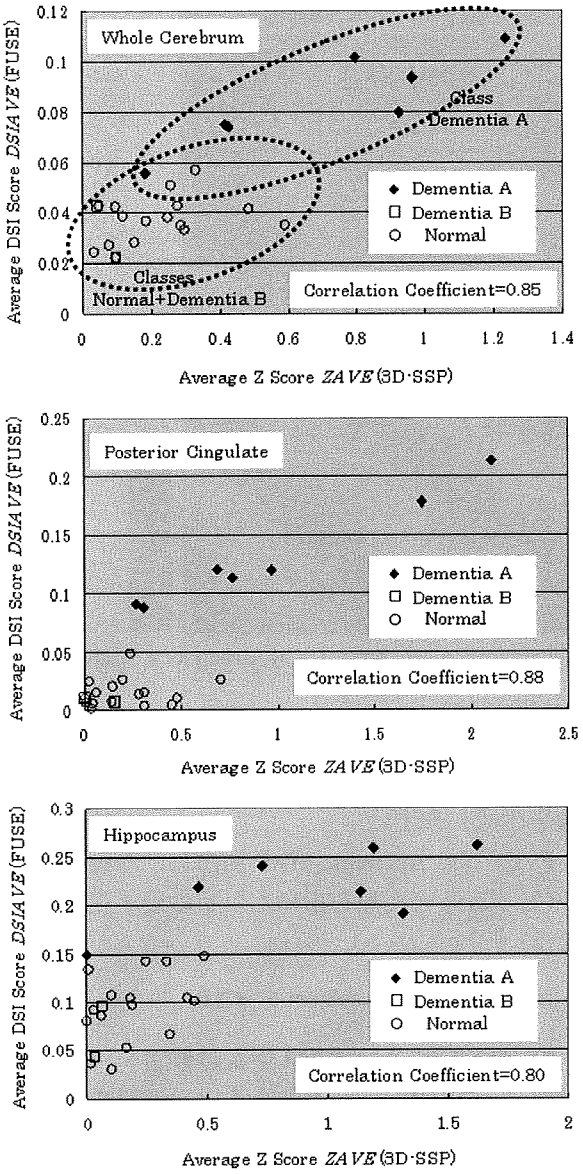

Fig. 2 Performance comparison of FUSE and 3D-SSP. The horizontal axis is the average Z-score per voxel in gray matter for 3-D SSP, and the vertical axis is the average DSI-score per voxel in gray matter for FUSE.

$$
\begin{aligned}
&f(\mathbf{x}) = L(\mathbf{x}) + U(\mathbf{x}) \\
&L(\mathbf{x}) = \sum_{i=1}^{m}[\sum_{j=1}^{n} a_{ij}x_j - b_i \log(\sum_{j=1}^{n} a_{ij}x_j)] \\
&U(\mathbf{x}) = \beta \sum_{(j,j')\in C} \omega_{(j,j')}(x_j - x_{j'})^2
\end{aligned}
\tag{6}
$$

ただし，$L(\mathbf{x})$はポアソン分布の対数尤度，$U(\mathbf{x})$は画像の平滑化を行うギブスの事前情報，C はクリークと呼ばれる隣接画素対の集合を表す．Anatomic-MAP 法では，MRI 画像から作成したテンプレート画像$\mathbf{m} = (m_1, m_2, \cdots, m_n)$を用いて，式

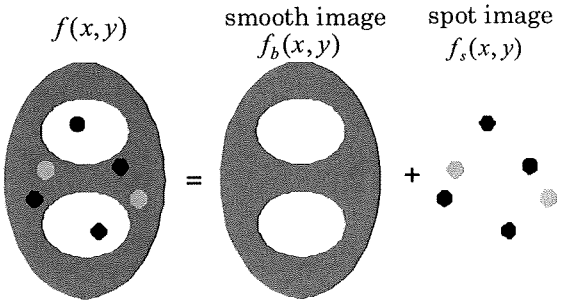

Fig. 3 Spots on smooth (SOS) image model.

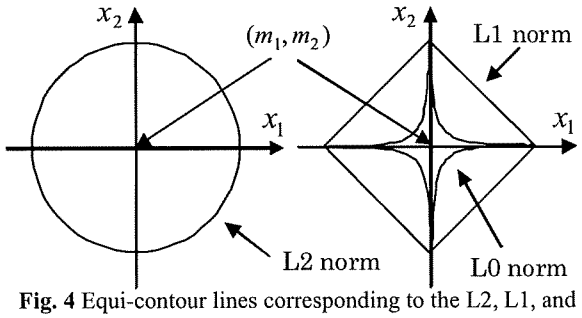

Fig. 4 Equi-contour lines corresponding to the L2, L1, and L0 norms.

(6) に以下の 2 つの修正を施した評価関数を用いる．まず，評価関数にテンプレート画像と再構成画像の距離$D(\mathbf{x})$を加え

$$
\begin{aligned}
&f(\mathbf{x}) = L(\mathbf{x}) + U(\mathbf{x}) + D(\mathbf{x}) \\
&D(\mathbf{x}) = \gamma \sum_{j=1}^{n} d(x_j, m_j)
\end{aligned}
\tag{7}
$$

とする．ただし，$d(a,b)$はaとbの距離を表す一変数関数である．次に，式 (6) のギブスの事前情報$U(\mathbf{x})$において，平滑化を行うクリークを同一領域内のクリーク$C \cap M$（Mは同一領域内に含まれる画素対の集合）に限定する．これらの修正により，1) テンプレート画像との距離が小さくなるように再構成されること，2) 領域境界のエッジを保存して同一領域内のみで平滑化されること，の 2 つの効果が期待される．

$d(a,b)$の形は再構成画像に大きな影響を及ぼす．SPECT ／ PET に限定せず従来の CT 画像再構成の研究では，具体的な$d(a,b)$の形として

$$
\begin{aligned}
&d(a,b) = (a-b)^2 \quad \text{(L2 norm)} \\
&d(a,b) = b\log(b/a) - b + a \quad \text{(Gamma prior)} \\
&d(a,b) = a\log(a/b) - a + b \quad \text{(Cross entropy)}
\end{aligned}
\tag{8}
$$

が使用されている．しかし，後述するように，これらの距離ではスポットのコントラストを保存

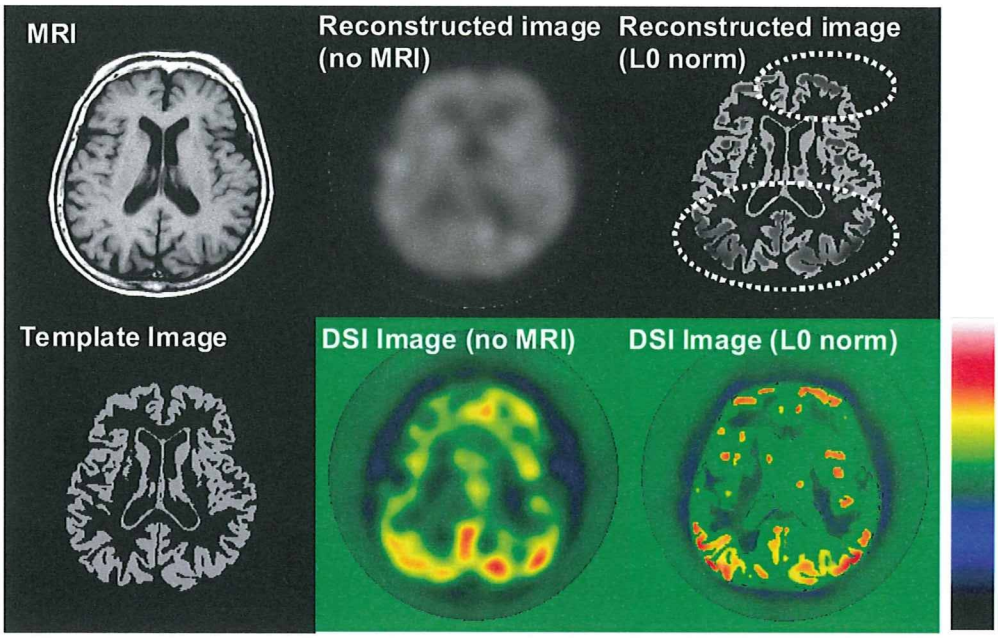

Fig. 5 Reconstructed images and DSI images obtained from SPECT projection data for a case of Alzheimer's disease.

し濃度の平坦部のみを平滑化する目的をほとんど達成できない．本研究では，$d(a,b)$として

$$\begin{aligned} d(a,b) &= |a-b| \quad \text{(L1 norm)} \\ d(a,b) &= \lim_{\varepsilon \to +0} |a-b|^{\varepsilon} \quad \text{(L0 norm)} \end{aligned} \tag{9}$$

を採用している．式 (9) が式 (8) と比較して優れている理由は，疎物体の画像再構成に対する文献〔7〕と同様に以下のように説明できる．簡単のため，未知数が 2 つ(x_1, x_2)の場合について L2 ノルム・L1 ノルム・L0 ノルムの距離$D(\mathbf{x})$の等値線を描くと，**Fig. 4** のようになる．ここで，(x_1, x_2)の一方がスポットで一方が正常部に相当する解は座標軸上（$x_1 = m_1$ または $x_2 = m_2$）にある場合に相当するが，L2 ノルムは等値線が同心円であるため座標軸上以外の点を解として選びやすくなる．これはスポットと正常部を平均化した解を選ぶことに相当し，スポットと正常部の境界は保存されない．これに対して，L1 ノルム・L0 ノルムでは座標軸から離れた点のコストを重く評価し，座標軸に近い解をより選びやすくなる．以上の説明は未知数が 2 つの場合であるが，多変数の場合も同様の議論が成り立ち，L1 ノルム・L0 ノルムは L2 ノルム（や他の式 (8) の距離）と比較してスポットと正常部の違いを強調した画像を生成しやすい．

以上から，Anatomic-MAP 法における画像再構成は，式 (9) の距離を用いた以下の最小化問題となる．

$$\text{minimize } f(\mathbf{x}) \quad \text{subject to } \mathbf{x} \geq 0 \tag{10}$$

3）Anatomic-MAP-EM 逐次近似法

次に，式 (10) の解を求める逐次近似法について述べる．本研究で提案する式 (9) の距離は微分不可能でかつ狭義凸関数でもないため，式 (8) のように微分可能な最適化の枠組みで取り扱うことができない．そこで，式 (9) の距離をうまく扱うことが可能な通常の MAP-EM 法の一反復とテンプレート画像 **m** に画素値を近づける濃度しきい値処理を交互に行う逐次近似法を開発した．ページ数の制約からこの逐次近似法について述べる余裕はないが，原著論文の文献〔6〕や本研究を発展させた文献〔8〕に詳しい説明がある．

実 SPECT 投影データと MRI 画像を用いて評価実験を行った．SPECT 撮影に用いた放射性薬剤は ^{123}I-IMP，投影データのサンプリングは 128（方向）× 128（検出器）である．**Fig. 5** に，L0 ノルムを用いた本手法による再構成画像と DSI 画像を示す．このデータはアルツハイマー病の症例で，脳の萎縮を伴わずに血流が低下している病変が

頭頂葉と後部帯状回に存在することが3D-SSPにより確認できたものである．部分容積効果はほぼ完全に補正され，MRI 画像に全く写っていない病変のコントラストと分解能も大きく改善され，病変が検出しやすい画像が生成されている．

最後に，SPECT／PET の画像再構成に MRI／CT の形態画像を利用する研究はいくつか存在するが〔9～11〕，上述のように形態画像に全く写っていない病変を強調する効果がある手法は，筆者が知る限り本手法と相互情報量（結合エントロピー）を用いた文献〔11〕の手法のみである．

4. まとめ

本論文では，同一患者のSPECT画像とMRI画像を融合して用い，脳の萎縮を伴わずに血流が低下している部位を検出する新しい脳血流画像解析手法FUSEを紹介した．また，同一患者のMRI画像を事前情報として巧妙に利用して，SPECT の主要な画質劣化要因である部分容積効果や統計雑音の影響を軽減し病変を検出しやすい画像を生成する新しい統計的画像再構成法を紹介した．私が最近行った研究の中でこれらのテーマはもっとも夢中になったものであり，今後も実用化を目指してさらなる改良や評価を行いたい．

謝　辞

本論文の内容の多くは，野村昌弘氏・豆生田友里氏・武田遼氏（筑波大学大学院），朝田隆教授（筑波大学），武田徹教授（北里大学），との共同研究である．また，本村信篤氏（東芝メディカルシステムズ）と北村圭司氏（島津製作所）には多大なご協力とご助言をいただいた．以上の方々に深謝いたします．

文　献

〔1〕 Minoshima S, Frey KA, Koeppe RA et al: Diagnostic approach in Alzheimer's disease using three-dimensional stereotactic surface projections of fluorine-18-FDG. J Nucl Med **36**: 1238-1248, 1995

〔2〕 Friston KJ, Ashburner JT, Kiebel SJ et al: Statistical parametric mapping: the analysis of functional brain images. Academic Press, 2006

〔3〕 松田博史，朝田　隆：見て診て学ぶ痴呆の画像診断．永井書店，2004

〔4〕 Kudo H, Nomura M, Asada T et al: Image processing method for analyzing cerebral blood-flow using SPECT and MRI. 2007 IEEE Medical Imaging Conference, Paper No. M19-399, 2007

〔5〕 Kudo H, Asada T, Takeda T: Analyzing cerebral blood-flow SPECT images for the diagnosis of dementia: a new approach FUSE. Med Imag Tech **26**: 169-174, 2008

〔6〕 Mameuda Y, Kudo H: New anatomical-prior-based image reconstruction method for PET/SPECT. 2007 IEEE Medical Imaging Conference, Paper No. M23-2, 2007

〔7〕 Li M, Yang H, Kudo H: An accurate iterative reconstruction algorithm for sparse objects: application to 3-D blood-vessel reconstruction from a limited number of projections. Phys Med Biol **47**: 2599-2609, 2002

〔8〕 小林哲哉，工藤博幸：PET／SPECT における画像再構成と病変検出の統合．Med Imag Tech **26**: 233-239, 2008

〔9〕 Sasty S, Carson RE: Multimodality Bayesian algorithm for image reconstruction in positron emission tomography: a tissue composition model. IEEE Trans Med Imaging **6**: 750-761, 1997

〔10〕 Baete K, Nuyts J, Paesschen WV et al: Anatomical-based FDG-PET reconstruction for the detection of hypo-metabolic regions in epilepthy. IEEE Trans Med Imaging **23**: 510-519, 2004

〔11〕 Nuyts J: The use of mutual information and joint entropy for anatomical priors in emission tomography. 2007 IEEE Medical Imaging Conference, Paper No. M23-3, 2007

工藤博幸（くどう　ひろゆき）

1985 年東北大・工・通信卒．1990 年同大大学院博士課程了．現在，筑波大・システム情報・教授．1990 年電子情報通信学会論文賞，1991 年・2001 年・2006 年・2008 年日本医用画像工学会論文賞，2006 年・2008 年国際雑誌『Inverse Problems 』High Lights，2008 年国際雑誌『Physics in Medicine and Biology』High Lights 受賞．工博．CT と PET を中心とした医用イメージング，画像処理の研究に従事．IEEE，電子情報通信学会，各会員．2008 年に CT の未解決問題である Interior Problem の安定な厳密解法を発見し，これに関する 2 つの論文が国際雑誌『Physics in Medicine and Biology』と『Inverse Problems』の 2008 High Lights を受賞した．

「電子ジャーナルでは Fig. 1, 5 をカラーでご覧いただけます URL:http://www.jamit.jp」

*　　*　　*

Intracortical Microcirculatory Change Induced by Anesthesia in Rat Somatosensory Cortex

Kazuto Masamoto, Takayuki Obata, Iwao Kanno

Molecular Imaging Center, National Institute of Radiological Sciences, Chiba, 263-8555, Japan, masamoto@nirs.go.jp

Abstract The present study aimed to characterize microcirculatory responses to anesthesia in brain tissue. With multi-photon excitation fluorescence microscopy, intra-cortical capillary dimension and red blood cell (RBC) flow were successfully visualized up to a depth of ~0.6 mm from the cortical surface in rats anesthetized with either isoflurane or α-chloralose. We observed that the diameter of the major cerebral artery was ~100 μm under isoflurane, but only ~75 μm under α-chloralose. At the same time, capillary diameter was observed to be slightly larger under α-chloralose than isoflurane: 5.1 ± 1.2 μm vs. 4.8 ± 1.1 μm, respectively. A significant difference in the mean RBC speed measured in single capillaries was observed: 0.4 ± 0.4 mm/sec under α-chloralose vs. 1.5 ± 0.4 mm/sec under isoflurane. In agreement with these observations, arterio-venous transit-time and laser-Doppler flowmetry consistently showed a significant reduction of the RBC and plasma blood speed under α-chloralose relative to isoflurane. These findings may indicate that local blood flow regulatory mechanisms exist at the capillary level for the balance of oxygen supply and demand induced by anesthesia in the brain tissue.

1 Introduction

A variety of brain tissue oxygen levels have been observed in animals under general anesthesia [1]. The direct and indirect effects of anesthesia involve the degree of anesthetic action on cerebral metabolic rate of oxygen ($CMRO_2$) and cerebral blood flow (CBF).

In a previous study, we found that rodents treated with inhalation anesthetics (e.g., isoflurane) or intravenous anesthetics (e.g., α-chloralose) that are widely used for brain activation studies, showed quite different behaviors for the activation-induced cortical hemodynamics [2]. Since hemodynamic-based brain imaging techniques rely on the microcirculatory responses to local neural activity, the effects of anesthesia on the brain microcirculation are critically important for

valid interpretation of neural functions. However, the effects of anesthesia on the brain microcirculation, such as vessel dimension and red blood cell (RBC) flow remain unaddressed.

In the present study, we directly measured intracortical capillary dimension and RBC flow in the cerebral cortex of rats anesthetized with either volatile isoflurane or injectable α-chloralose. A biocompatible fluorescent dye was intravenously injected for visualization of blood plasma and cortical microvasculature was three-dimensionally visualized with in vivo multi-photon excitation fluorescent microscopy up to a depth of 0.6 mm from the cortical surface. Intraluminal vascular dimension and fluorescently labeled RBC speed were then measured.

2 Materials and Methods

All animal protocols were approved by the NIRS Animal Experiment Committee. The animals (250-350 g Sprague-Dawley rats, N = 9) were initially anesthetized with 4 to 5% isoflurane and maintained with 2% during surgical procedures. The animal was mechanically ventilated and physiologic parameters (e.g., end-tidal CO_2, anesthetic gas concentration, respiratory rate, heart rate, and mean arterial blood pressure) were monitored throughout all experiments. Arterial blood gas was periodically measured, and respiratory rate and minute ventilation volume were adjusted as needed. Rectal temperature was maintained at 37.0 ± 0.2 °C.

A portion of the left skull (3 mm by 3 mm) over the somatosensory area was removed. The opened area was filled with physiologic saline solution. For experiments, the anesthesia level was first maintained with isoflurane (~1.4%) and then switched to α-chloralose (45 mg/kg/h, i.v.), as previously reported [2]. For visualization of the cortical vasculature, a bolus of Qdot® 605 (1 μM in buffered solution, Invitrogen) was intravenously injected (0.2 to 0.4 ml). The cortical vasculature was then visualized with multi-photon excitation fluorescent microscope (TCS SP5, Leica Microsysems) with an excitation wavelength of 900 nm (MaiTai HP, Ti:Sapphire laser, Spectra-Physics). The objective lens was a ×20 water-immersion lens (0.5 NA, Leica Microsystems). The 512 pixel by 512 pixel images covered a cortical area of 456 μm by 456 μm with a pixel resolution of 0.89 μm. To obtain the three-dimensional structure, contiguous images were captured up to a depth of ~0.6 mm from the cortical surface with a step size of 0.01 mm in the z-direction. The region of interest was selected with care to avoid areas having vessels of a relatively large size at the cortical surface. A final image was taken to cover an area of 912 μm by 912 μm in the x-y plane by scanning four adjacent regions. For display purposes, a maximum-intensity projection was constructed from contiguous images obtained in the z-direction.

Based on their pulsation and branching geometry, arterial and venous networks were distinguished at the cortical surface, and then tracked into the pa-

renchyma tissue. To measure capillary diameter, a maximum intensity projection was created from every 0.1-mm thickness in the z-direction and then the width in the image was calculated. A single-capillary was defined as the single vessel part having cross-sectional thickness less than 8 μm and for which both edges continued to two new vessels as a branching.

The RBC speed was measured by tracking a FITC-labeled RBC through a single-capillary. Time-lapse images were obtained at a rate of 14 to 167 frames per second, depending on the number of lines to be scanned in each single frame. The scanning area was set to cover the whole structure of the single-capillary shape (i.e., 64 to 256 lines). Similarly, the speed of blood plasma was evaluated by tracking 0.1-μm diameter fluorescent beads that were intravenously injected. For the measurement of mean arterio-venous transit time, a bolus injection (0.1 ml) of fluorescently labeled RBCs or fluorescent beads was performed via the femoral vein. The time-lapse image was obtained with a 5x objective lens at a rate of seven frames per second. Statistical analysis was performed with a t-test.

3 Results

There was no detectable difference in the measured physiologic parameters (arterial blood gas and blood pressure) between isoflurane and α-chloralose conditions (Table 1). We observed that the diameter of the principal artery at the cortical surface was ~100 μm under isoflurane, but ~75 μm under α-chloralose. The results showed that the principal artery shrank significantly after induction with α-chloralose. However, the intracortical capillary diameter was slightly larger under α-chloralose (5.1 ± 1.2 μm, n = 1682 vessels) compared to the isoflurane condition (4.8 ± 1.1 μm, n = 1746 vessels). A statistically significant difference ($P < 0.05$) was observed between the two-conditions. These results indicate that the upstream and downstream vessels react differently depending on the anesthetics.

The mean RBC speed in a single capillary was significantly lower under α-chloralose relative to the isoflurane condition: 0.4 ± 0.4 mm/sec under α-chloralose vs. 1.5 ± 0.4 mm/sec under isoflurane. Under α-chloralose, some RBCs were found to be very slow (< 0.01 mm/sec), whereas most RBCs measured under isoflurane had a relatively high speed (0.4 to 3.0 mm/sec).

As expected, the arterio-venous transit-time of the labeled RBCs was significantly longer under α-chloralose (2.8 ± 1.7 sec at peak-to-peak) as compared to the isoflurane conditions (1.0 ± 0.9 sec). Similar results were observed for the transit-time of blood plasma: 1.8 ± 1.3 sec under α-chloralose and 1.2 ± 0.7 sec under isoflurane. These results clearly indicated that both RBC and plasma blood speed were significantly lower under α-chloralose relative to isoflurane conditions.

4 Discussion

It has been previously shown by other groups that the baseline CBF under α-chloralose was 30 to 50% lower than under isoflurane in rat somatosensory cortex, i.e. 70 to 90 mL/100 g/min under α-chloralose [3,4] vs. 130 to 150 mL/100 g/min under isoflurane [5,6]. In a previous study, we found the baseline CBF measured with laser-Doppler flowmetry was 31% lower under α-chloralose compared with isoflurane [2]. Our measurements of the arterial dimension are in good agreement with these literature data, indicating that the tone in the upstream resistance vessels has a significant role in the regulatory mechanism of the baseline CBF induced by anesthesia. However, we found that the effect of the anesthesia on the intracortical capillary diameter was opposite to the arterial response. Namely, a slightly larger capillary diameter was observed under α-chloralose as compared to the isoflurane condition. This might indicate that the upstream arteries and intracortical microvessels have separate or independent mechanisms for the regulation of local CBF.

Our results for the mean RBC speed consistently showed that the speed was significantly lower under α-chloralose relative to the isoflurane condition. These results are in good agreement with previous CBF data. However, the measured RBC speed under isoflurane was relatively high compared to the literature data. With a multi-photon microscope system, Kleinfeld et al. (1998) reported that the intra-cortical RBC speed was 0.77 mm/sec in rats anesthetized with urethane [7]. The ranges of RBC speed in capillaries were reported as 0.3 to 3.2 mm/sec [8]. In the present study, we showed that the variable speed of RBCs could be due to a local regulatory mechanism rather than upstream arterial regulation. Since the capillary volume and speed of RBCs critically affect oxygen transfer processes from nearby blood vessels to the energy consuming tissue site, it is worthwhile to compare the tissue oxygen level between both anesthesia conditions. Our group has reported that the mean tissue oxygen level in rat somatosensory cortex was 29 mmHg under α-chloralose and 33 mmHg under isoflurane [9,10]. Another study with electron paramagnetic resonance oximetry showed that the mean tissue oxygen level at normoxic conditions was 13 mmHg under a cocktail of α-chloralose and urethane and 38 mmHg under isoflurane [11]. The data from those studies were in good agreement with the CBF data; higher CBF produces a higher tissue oxygen level and vice versa. The anesthesia may affect the tissue oxygen metabolic rate in a different manner, and thus a possible scenario where the effect of anesthesia on the energy metabolism becomes a dominant factor leading to the observed difference in tissue oxygen level cannot be ruled out. However, it should be noted that endothelial cells have the ability to control their dimension by sensing the nearby blood oxygenation level [12], which may play a significant role in adjusting local oxygen demand and supply via regulation of capillary volume and RBC speed. Further studies are needed to elucidate

the full regulatory mechanism for the local regulation of the microvascular dimensions and RBC traffic.

Acknowledgments The authors thank Mr. Jeff Kershaw for critical reading of this manuscript. This work was partially supported by KAKENHI (#19800065).

References

[1] Ndubuizu, O., LaManna, J. C., 2007, Brain tissue oxygen concentration measurements, Antioxid Redox Signal. 9:1207-1219.

[2] Masamoto, K., Kim, T., Fukuda, M., Wang, P., Kim, S. G., 2007, Relationship between neural, vascular, and BOLD signals in isoflurane-anesthetized rat somatosensory cortex, Cereb Cortex. 17:942-950.

[3] Ueki, M., Linn, F., Hossmann, K. A., 1988, Functional activation of cerebral blood flow and metabolism before and after global ischemia of rat brain, J Cereb Blood Flow Metab. 8:486-494.

[4] Lee, S. P., Duong, T. Q., Yang, G., Iadecola, C., Kim, S. G., 2001, Relative changes ofcerebral arterial and venous blood volumes during increased cerebral blood flow: implications for BOLD fMRI, Magn Reson Med. 45:791-800.

[5] Maekawa, T., Tommasino, C., Shapiro, H. M., Keifer-Goodman, J., Kohlenberger, R. W., 1986, Local cerebral blood flow and glucose utilization during isoflurane anesthesia in the rat, Anesthesiology. 65:144-151.

[6] Lenz, C., Frietsch, T., Futterer, C., Rebel, A., van Ackern, K., Kuschinsky, W., Waschke, K. F., 1999, Local coupling of cerebral blood flow to cerebral glucose metabolism during inhalational anesthesia in rats: desflurane versus isoflurane, Anesthesiology. 91:1720-1723.

[7] Kleinfeld, D., Mitra, P. P., Helmchen, F., Denk, W., 1998, Fluctuations and stimulus-induced changes in blood flow observed in individual capillaries in layers 2 through 4 of rat neocortex, Proc Natl Acad Sci U S A. 95:15741-15746.

[8] Hudetz, A. G., 1997, Blood flow in the cerebral capillary network: a review emphasizing observations with intravital microscopy, Microcirculation. 4:233-252.

[9] Masamoto, K., Kershaw, J., Ureshi, M., Takizawa, N., Kobayashi, H., Tanishita, K., Kanno, I., 2007, Apparent diffusion time of oxygen from blood to tissue in rat cerebral cortex: implication for tissue oxygen dynamics during brain functions, J Appl Physiol. 103:1352-1358.

[10] Masamoto, K., Vazquez, A., Wang, P., Kim, S. G., 2008, Trial-by-trial relationship between neural activity, oxygen consumption, and blood flow responses, Neuroimage. 40:442-450.

[11] Hou, H., Grinberg, O. Y., Taie, S., Leichtweis, S., Miyake, M., Grinberg, S., Xie, H., Csete, M., Swartz, H. M., 2003, Electron paramagnetic resonance assessment of brain tissue oxygen tension in anesthetized rats, Anesth Analg. 96:1467-1472.

[12] Inoue, K., Tomita, M., Fukuuchi, Y., Tanahashi, N., Kobari, M., Takao, M., Takeda, H., Yokoyama, M., 2003, Dynamic observation of oxygenation-induced contraction of and transient fiber-network formation-disassembly in cultured human brain microvascular endothelial cells, J Cereb Blood Flow Metab. 23:821-828.

Table 1. Blood gas condition, mean arterial blood pressure (BP), and mean capillary diameter (Dc) observed under isoflurane and α-chloralose conditions (Mean ± SD, N = 9).

	*p*H	pCO_2 (mmHg)	pO_2 (mmHg)	BP (mmHg)	Dc (μm)
Isoflurane	7.43 ± 0.03	37 ± 3	128 ± 18	94 ± 11	4.8 ± 1.1
α-chloralose	7.44 ± 0.02	36 ± 2	123 ± 16	115 ± 15	5.1 ± 1.2

Journal of Cerebral Blood Flow & Metabolism (2010) 30, 187–195

www.jcbfm.com

Measurement error analysis for the determination of dopamine D_2 receptor occupancy using the agonist radioligand [^{11}C]MNPA

Miho Shidahara[1], Hiroshi Ito[2], Tatsui Otsuka[2], Yoko Ikoma[2,3], Ryosuke Arakawa[2], Fumitoshi Kodaka[2], Chie Seki[1], Harumasa Takano[2], Hidehiko Takahashi[2], Federico E Turkheimer[4], Yuichi Kimura[1], Iwao Kanno[1] and Tetsuya Suhara[2]

[1]*Biophysics Group, Molecular Imaging Center, National Institute of Radiological Sciences, Chiba, Japan;* [2]*Molecular Neuroimaging Group, Molecular Imaging Center, National Institute of Radiological Sciences, Chiba, Japan;* [3]*Department of Investigative Radiology, National Cardiovascular Center Research Institute, Osaka, Japan;* [4]*Department of Clinical Neuroscience, Division of Neuroscience and Mental Health, Imperial College London, London, UK*

The purpose of this study is to investigate errors in quantitative analysis for estimating dopamine D_2 receptor occupancy of antipsychotics with agonist radioligand [^{11}C]MNPA by numerical simulation, with particular attention to the validity of a quantitative approach based on the use of a reference region. Synthetic data were validated using clinical data combined with a bootstrap approach. Time–activity curves (TACs) of [^{11}C]MNPA were simulated, and the reliability of binding potential (BP_{ND}) and occupancy estimated by nonlinear least square (NLS) fitting and a simplified reference tissue model (SRTM) were investigated for various noise levels and scan durations. In the human positron emission tomography (PET) study with and without antipsychotic, risperidone, the uncertainty of BP_{ND} and occupancy estimated by SRTM was investigated using resampled TACs based on bootstrap approach with weighted residual errors of fitting. For both NLS and SRTM, it was possible to have <3% of bias in occupancy estimates of [^{11}C]MNPA by 60 mins. However, shortened scan duration degrades the quantification of very small binding potentials, especially in case of SRTM. Observations were replicated on the clinical data. Results showed that dopamine D_2 receptor occupancy by antipsychotics can be estimated precisely in region of interest analysis by SRTM with a longer than 60-min [^{11}C]MNPA PET scan duration.
Journal of Cerebral Blood Flow & Metabolism (2010) **30,** 187–195; doi:10.1038/jcbfm.2009.193; published online 16 September 2009

Keywords: positron emission tomography; dopamine D_2 receptor; occupancy; [^{11}C]MNPA; bootstrap; reference region

Introduction

The dopamine D_2 receptor exists in both high- and low-affinity states, and the state of high affinity for endogenous dopamine is defined as the functionally active form of the receptor. To determine the binding to the high-affinity state of dopamine D_2 receptors, agonist ligands have been developed (Jones *et al*, 1984; Neumeyer *et al*, 1973). It has been reported that [^{11}C]-(R)-2-CH_3O-*N*-*n*-propylnorapomorphine ([^{11}C]MNPA), one of the agonist radioligands, is more sensitive than conventional D_2 antagonist radioligands [^{11}C]raclopride to the displacement of binding by endogenous dopamine, thus proposing [^{11}C]MNPA as promising radioligand for positron emission tomography (PET) imaging of the high-affinity state of dopamine D_2 receptors in the primate brain (Seneca *et al*, 2006).

The dopamine D_2 receptor is a main therapeutic target in schizophrenia, and most antipsychotics have an antagonistic action toward dopamine D_2 receptors. Occupancy of dopamine D_2 receptors evoked by competition from antipsychotic medication can be estimated from the reduction in the observed binding potential (BP_{ND}) (Farde *et al*, 1988; Farde *et al*, 1990). Several quantitative methods have been proposed for estimating BP_{ND}, and a simplified

Correspondence: Dr H Ito, Molecular Neuroimaging Group, Molecular Imaging Center, National Institute of Radiological Sciences, Anagawa 4-9-1, Inage, Chiba 263-8555, Japan.
E-mail: hito@nirs.go.jp
Received 27 May 2009; revised 10 August 2009; accepted 11 August 2009; published online 16 September 2009

reference tissue model (SRTM) (Lammertsma and Hume, 1996) has often been used. The SRTM uses as input the time activity of a reference brain region with negligible specific binding and therefore avoids arterial blood sampling. As an occupancy study requires two PET scans, elimination of arterial blood sampling by SRTM method has practical appeal.

Otsuka *et al* (2009) showed that the SRTM method can be applied to human [^{11}C]MNPA for quantitative BP_{ND} estimation; however, a precise quantitative evaluation of the SRTM method for occupancy studies with [^{11}C]MNPA has not yet been performed. However, error analysis is important to ascertain whether the variability in occupancy with antipsychotics measured [^{11}C]MNPA is truly biological or generated by the PET measurement system. In this regard, Yokoi *et al* reported that occupancy levels of the partial agonist aripiprazole, a new antipsychotic a partial agonist for dopamine D_2 receptors without notable extrapyramidal side effects, vary widely, contrasting with the usual presence of extrapyramidal side effects at occupancy levels exceeding 80% for D_2 antagonists (Farde *et al*, 1988; Kessler, 2007; Yokoi *et al*, 2002). It is therefore of relevance to perform an error analysis of BP_{ND} estimation for PET dynamic scanning with [^{11}C]MNPA to quantify the variability induced by the measurement itself to better appreciate the biological variability that may emerge from human bioassays that use this tracer.

In this study, we simulated and evaluated errors in the quantitative analysis for the estimation of dopamine D_2 receptor occupancy when measured with [^{11}C]MNPA with particular attention to the use of SRTM. The effect of scan duration on the error of estimates was also evaluated, because shorter scan duration reduces patient's burden. Tissue kinetics where simulated using a compartmental model and, to assess model validity, we compared the results of the simulations with the errors obtained from clinical data by use of a resampling technique.

Materials and methods

Kinetics of [^{11}C]MNPA

The kinetics of [^{11}C]MNPA in the brain is based on the two-tissue three-compartment model as follows:

$$\begin{aligned}\frac{dC_{ND}(t)}{dt} &= K_1 C_P(t) - (k_2 + k_3)C_{ND}(t) + k_4 C_S(t)\\ \frac{dC_S(t)}{dt} &= k_3 C_{ND}(t) - k_4 C_S(t)\\ C_T(t) &= C_{ND}(t) + C_S(t)\end{aligned} \quad (1)$$

where C_P [Bq/mL] is the radioactivity concentration of unchanged radioligand in plasma (arterial input function), C_{ND} [Bq/cm^3] is the radioactivity concentration of nondisplaceable radioligand in brain, including nonspecifically bound and free radioligand, and C_S [Bq/cm^3] is the radioactivity concentration of radioligand specifically bound to receptors. The rate constants K_1 [mL/cm^3/min] and k_2 [min^{-1}] represent the influx and efflux rates for radioligand diffusion through the blood–brain barrier. The rate constants k_3 [min^{-1}] and k_4 [min^{-1}] represent the radioligand transfers between the compartments for nondisplaceable and specifically bound radioligand. C_T [Bq/cm^3] is the radioactivity concentration in a brain region measured by PET.

Estimation of receptor occupancy

Nonlinear least squares fitting for BP_{ND}: K_1, k_2, k_3, and k_4 values in Equation (1) can be determined by nonlinear least squares (NLS) fitting of the time–activity curve (TAC) in the target region. The cerebellum is regarded as a reference region because this brain structure has negligible D_2 dopamine receptor density (Otsuka *et al*, 2009; Seneca *et al*, 2008; Tokunaga *et al*, 2009). K_1^r and k_2^r values in the cerebellum were also determined by NLS using the one-tissue compartment model without the specific binding compartment. The BP_{ND} can be expressed using the reference region as:

$$BP_{ND} = \frac{(K_1/k_2)(k_3/k_4 + 1)}{(K_1^r/k_2^r)} - 1 \quad (2)$$

where $(K_1/k_2)(k_3/k_4 + 1)$ is the total distribution volume of the target region and (K_1^r/k_2^r) is that of the cerebellum. In this study, the calculation of BP_{ND} in Equation (2) was regarded as the standard method for BP_{ND} estimation (Otsuka *et al*, 2009). It should be noted that to improve the stability of the NLS fitting for target regions, the K_1/k_2 ratio for the target region was assumed to be the value in the cerebellum (K_1^r/k_2^r) as obtained by NLS using the one-tissue compartment model, meaning that, as a result, BP_{ND} in Equation (2) is equivalent to k_3/k_4 in this study.

Simplified reference tissue model for BP_{ND}: The SRTM yields the binding potential value by eliminating the arterial input function, C_P, arithmetically from model equations by using a TAC from a reference region where specific bindings are negligible, under the assumptions that the distribution volume of the nondisplaceable compartment was equal in the target and reference regions, and that a target region can be described with the one-tissue compartment model shown in Equation (3) (Lammertsma and Hume, 1996).

$$\begin{aligned}C_T(t) &= R_1 \cdot C_R(t) + \left(k_2 - \frac{R_1 k_2}{1 + BP_{ND}}\right) \cdot e^{\left(-\frac{k_2}{1+BP_{ND}}t\right)} \otimes C_R(t)\\ R_1 &= K_1/K_1^r\end{aligned} \quad (3)$$

where C_T and C_R are the radioactivity concentrations in the target and reference regions, respectively. The SRTM estimates three parameters, the delivery ratio of the target region to reference region (R_1), the clearance rate constant of the target region (k_2), and binding potential, referred to as BP_{ND} by nonlinear least squares.

Receptor occupancy: Receptor occupancy is calculated from BP_{ND} of two scans, with and without antipsychotics, as follows:

$$Occupancy\ (\%) = 100 \cdot (BP_{control} - BP_{drug})/BP_{control} \quad (4)$$

where $BP_{control}$ represents the BP_{ND} value derived from a scan without drug and BP_{drug} represents that from a scan with drug (Farde *et al*, 1988).

Simulation study

To evaluate the dependency of the noise level and scan duration for the estimated BP_{ND} and occupancy, we performed the following simulations. Both NLS and SRTM procedures were performed using in-house software written in the C program with downhill simplex algorithm (Nelder and Mead, 1965) without weighting and without constraints for the range of estimated parameters.

Time–activity curves for [^{11}C]MNPA: A dynamic tracer concentration for [^{11}C]MNPA was derived from the kinetic parameters listed in Table 1 with a dynamic frame (20 secs × 9, 1 min × 5, 2 mins × 4, 4 mins × 11, 5 mins × 6, total 90 mins) and a measured arterial input function (10 secs × 12, 30 secs × 2, 60 secs × 7, 120 secs × 1, 180 secs × 1, 300 secs × 3, 600 secs × 6, total 90 mins) of a single subject obtained by Otsuka *et al* (2009). These K_1, k_2, and k_4 were estimated based on the two-tissue three-compartment model using NLS fitting of region of interests (ROIs) in the putamen at baseline (the number of subjects (n) = 10) (Otsuka *et al*, 2009). Furthermore, three k_3 values, 0.015, 0.075, and 0.15, were arbitrarily chosen to investigate the occupancy of antipsychotics with [^{11}C]MNPA. During a loading study with a drug, the observed binding potential (BP_{ND}) is reduced mainly due to the suppression of the radioligand transfers from the compartments for nondisplaceable to specifically bound radioligand, k_3. Therefore, we varied k_3 values while covering the practical range of occupancy from a likely level at 50% to the extreme scenario of a 90% occupancy. A measured arterial plasma input function of a single subject according to human PET imaging protocols and noise-free simulated TACs (three target curves and a reference) are shown in Figure 1A and B.

Noise was generated with random generator based on Gaussian distribution and added to the decay-corrected target TACs. The noise ratio for each time frame was determined (Ikoma *et al*, 2008) according to the collected total count given by

$$NOISE_i(\%) = \left(\sqrt{N_i}/N_i\right) \cdot 100$$
$$N_i = \int_{t_i-\frac{\Delta t_i}{2}}^{t_i+\frac{\Delta t_i}{2}} C_T(t) \cdot e^{-\lambda t} dt \cdot F \quad (5)$$

where i is the frame number, C_T is the decay-corrected tissue radioactivity concentration derived from the k-values and the input function, t_i is the midpoint time of the i-th frame, Δt_i is the data collection time, λ is the radioisotope decay constant, and F is a scaling factor representing the sensitivity of the measurement system and is introduced here for adjusting the noise level.

Noise level dependency: Target TACs of [^{11}C]MNPA with several noise levels were generated to investigate the bias and variation of parameter estimates caused by the statistical noise for NLS and SRTM. The bias and variation were calculated as %bias of estimated BP_{ND} against the true BP_{ND} value and coefficient of variance (COV) by the mean and s.d. of the estimates excluding the outliers, respectively.

In this simulation study, the noise level for dynamic data was expressed as the mean of percentage noise described in Equation (5) from 1 to 90 mins, and it was chosen so that the mean of percentage noise would be 1%, 3%, 5%, 7%, and 10%, with 500 noisy data sets being generated for each. An example of noise-added simulated TAC with $BP_{ND} = 0.417$ is shown in Figure 1C.

In these noise-added TACs, each kinetic parameter including BP_{ND} was estimated by NLS and SRTM with a noise-free reference TAC. For both NLS and SRTM, initial parameters varied by ±25% from the true value (Ichise *et al*, 2003; Ikoma *et al*, 2008), and parameter estimates were considered invalid outliers if estimated parameters were negative or more than three times the true value (Ichise *et al*, 2003; Ikoma *et al*, 2008). Occupancy was also calculated from Equation (4) by using estimated BP_{ND} with assumed $k_3 = 0.15$ as $BP_{control}$ and with assumed $k_3 = 0.015$ or 0.075 as BP_{drug}.

Scan duration: The effect of scan duration on BP_{ND} and occupancy estimates was investigated for both NLS and SRTM methods. In the 90-min simulated TACs of 3% noise level corresponding to the noise level of human ROI analysis, the duration of the scan used for the parameter estimation was progressively reduced from 90 to 32 mins (32, 44, 60, 75, and 90 mins) for [^{11}C]MNPA.

Table 1 Kinetic parameters for the simulation study of [^{11}C]MNPA

	K_1	k_2	k_3	k_4	BP_{ND}	Occup. (%)
Target regions	0.44	0.067	0.015	0.18	0.0833	90
			0.075		0.417	50
			0.15		0.833	—
Reference region	0.44	0.067	—	—	—	—

Human study

Subjects and positron emission tomography procedure: [^{11}C]MNPA PET studies were performed before and after antipsychotic drug administration of risperidone (0.5 and 2.0 mg) on separate days for each two healthy male volunteers (20 to 21 y.o.). Scan start time after antipsychotic administration was 4 h. The study was approved by the ethics and radiation safety committees of the National

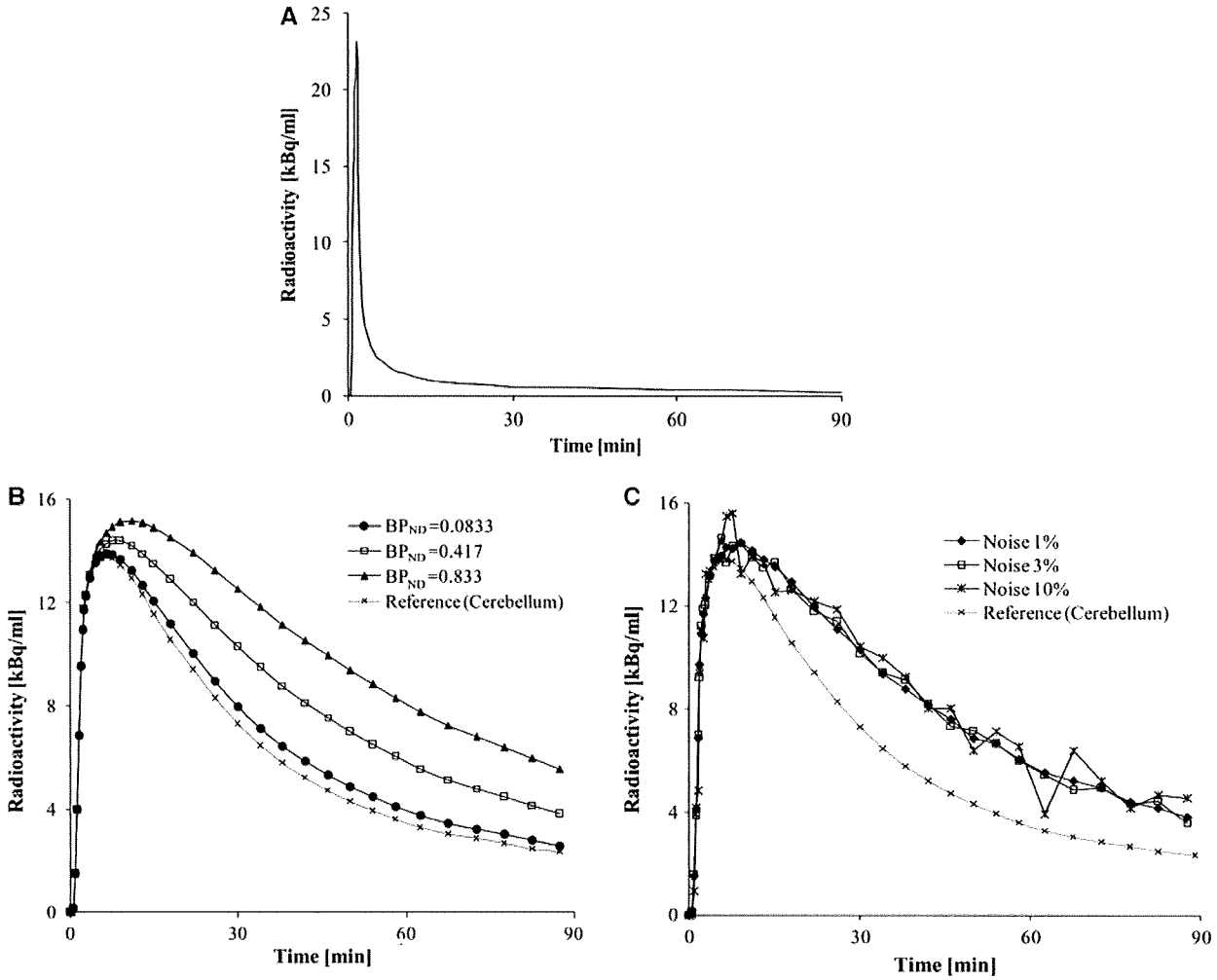

Figure 1 (**A**) Metabolite-corrected plasma input function of a single normal subject for simulation study. (**B**) Noise-free simulated TACs of three BP_{ND} values and reference TAC. (**C**) Noise-added TACs in the case of $BP_{ND} = 0.417$.

Institute of Radiological Sciences, Chiba, Japan. Written informed consent was obtained from each subject.

The PET acquisitions were performed on the ECAT EXACT HR+ (CTI-Siemens, Knoxville, TN, USA). A 10-min transmission scan with 3-rod source of ^{68}Ge–^{68}Ga was performed. Dynamic PET scans of [^{11}C]MNPA were performed for 90 mins in three-dimensional mode with a bolus injection of 208.0 to 234.0 MBq. Frame intervals were the same as this simulation study. The specific radioactivity was 245.1 to 313.8 GBq/μmol at the time of injection. Arterial blood sampling was not performed. All emission data were reconstructed by filtered-back projection using a Hanning filter with a cut-off frequency of 0.4.

Data analysis: The summed PET images for all frames were coregistered to individual MR images, and ROIs were drawn manually over the putamen, caudate, and cerebellum. Especially, R_1, k_2, and BP_{ND} in the putamen were estimated by SRTM using the cerebellum as reference region.

Human data were used to check model validity for the simulation studies. Given that an occupancy is measured only once (two scans for subject) and that repetitive measurements are not usually available, the reliability of parameter estimates can be evaluated by a bootstrap approach with weighted residual errors of fitting as published earlier (Rosso *et al*, 2009; Turkheimer *et al*, 1998). For each ROI in each individual subject data, 500 replication TACs were generated using bootstrap approach, and then parameters were estimated by SRTM and the COV of these 500 estimates was calculated to produce an accurate estimate of the statistical variability of the parameters. The weighted residual, ξ, using model-predicted tissue TAC, C_T, and the measured tissue TAC, X, were calculated as follows;

$$\begin{aligned} \xi_i &= (X(t_i) - C_T(t_i)) \cdot \sqrt{N_i} \\ N_i &= \int_{t_i - \frac{\Delta t_i}{2}}^{t_i + \frac{\Delta t_i}{2}} C_T(t) \cdot e^{-\lambda t} dt \end{aligned} \quad (6)$$

Then the residuals, $\{\xi_i\}$ $(i = 1, \ldots, k)$, were randomly resampled with substitution into a new set of the residuals

$\{\xi_i^*\}$. As an example with $k=5$, $[\xi_1, \xi_2, \xi_3, \xi_4, \xi_5]$ were randomly selected $[\xi_5, \xi_1, \xi_4, \xi_1, \xi_3]$ as a new residual set $[\xi_1^*, \xi_2^*, \xi_3^*, \xi_4^*, \xi_5^*]$. The bootstrapped residuals were used to generate a new data X^* defined as,

$$X^*(t_i) = C_T(t_i) + \frac{\xi_i^*}{\sqrt{N_i}} \quad (7)$$

In keeping with the simulation study, the relationship between the scan duration and COV of estimates and between the scan duration and bias was investigated by shortening the interval of fitting of the bootstrap replication TACs from 90 to 32 mins. The bias of BP_{ND} and occupancy was defined as the difference between the mean of these calculated for each truncated fitting interval and that of the 90 mins. Parameter estimates based on bootstrap approach were considered invalid outliers if estimates from X^* were negative or more than three times that of the 90 mins.

Results

Simulation study

Noise level dependency: In the NLS method, the bias of BP_{ND} was small especially at a low noise level. However, COV of BP_{ND} became larger as the noise level increased (Figure 2A). In the SRTM method, the bias of BP_{ND} was observed even though TACs were free from noise and both the bias and COV of BP_{ND} became larger as the noise increased, which is typical in the case of small BP_{ND} (Figure 2B). For both NLS and SRTM methods, these bias and COV values of occupancy were smaller compared with BP_{ND}. The tendency that COV with 90% occupancy was smaller compared with that with 50% occupancy was a common observation for NLS and SRTM.

Scan duration: The relationship between the reliability of BP_{ND} and occupancy estimates and the scan duration was investigated as shown in Figure 3. The bias of BP_{ND} and occupancy estimated by NLS was small despite short scan durations (Figure 3A); however, more than 10% outliers was caused with $BP_{ND}=0.0833$ at 32, 44, 60, 75, and 90 mins (Table 2). As scanning time became shorter, BP_{ND} for all three conditions was overestimated by SRTM (Figure 3B) and its bias magnitude was larger than that of NLS. More than 10% outliers was seen with $BP_{ND}=0.0833$ at 32 and 44 mins, $BP_{ND}=0.417$ at 32 mins and 0.833 at 32 mins. Bias was under 3% at a 3% noise level with occupancy estimates by SRTM method with scan duration longer than 60 mins (Figure 3B).

Human study

Time–activity curves: As shown in Figure 4, the shape of the TACs was similar between before and after antipsychotic administration in the cerebellum, whereas the accumulation of radioactivity in the postantipsychotic scan decreased at late times in other regions. In Figure 4A and B, estimated BP_{ND} in putamen of a subject before and after administration of Risperidone 2 mg were 0.968 and 0.437, then its occupancy resulted in 54.8%. For the other subject shown in Figure 4C and D, estimated BP_{ND} in putamen of a subject before and after administration

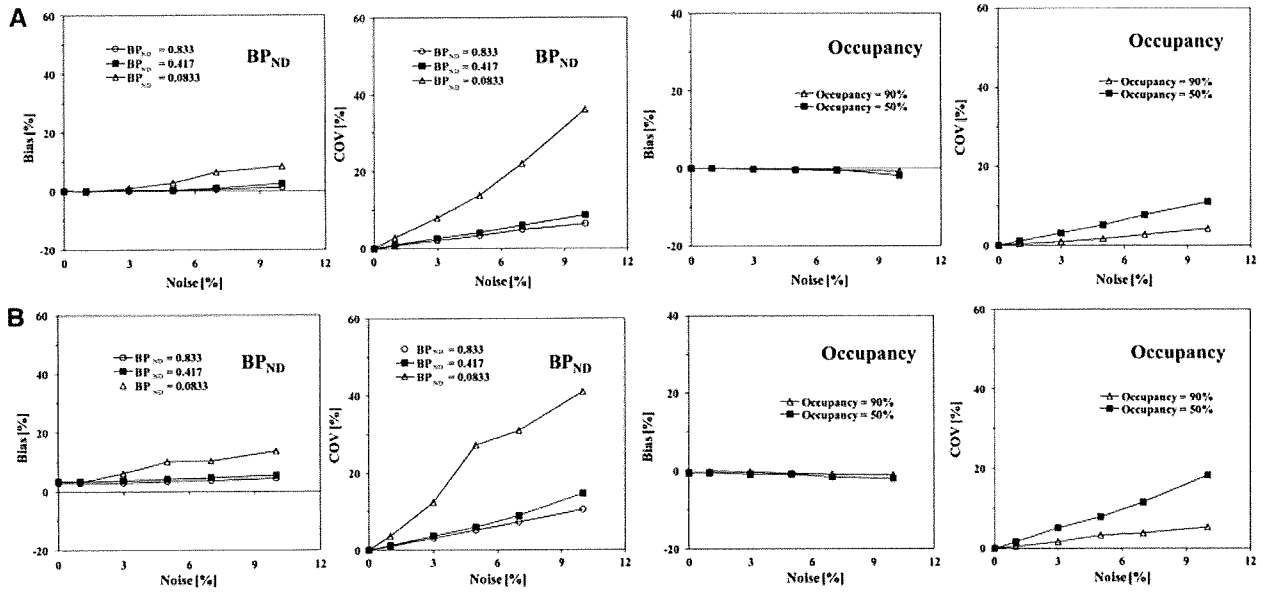

Figure 2 Noise level dependency. (**A**) Bias and COV of BP_{ND} and occupancy estimated by NLS ($K_1/k_2 = 6.6$ fixed), (**B**) estimated by SRTM.

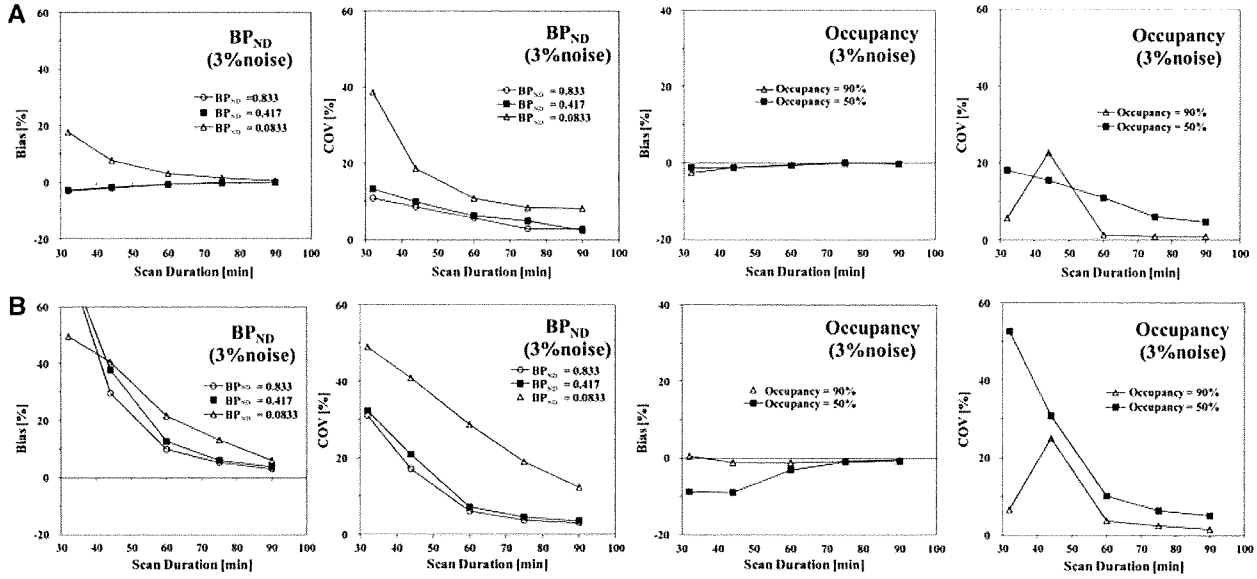

Figure 3 Scan duration dependency of bias and COV of BP_{ND} and occupancy at a 3% noise level estimated by (**A**) NLS and (**B**) SRTM methods.

Table 2 Scan duration dependency on the percentages of outliers of BP_{ND} at 3% noise level estimated by NLS and SRTM

	BP_{ND}	*Scan duration (min)*				
		32	*44*	*60*	*75*	*90*
NLS	0.0833	27.4	22.8	22.6	12.8	10.8
	0.417	5.8	3.4	1.4	2.6	1.2
	0.833	3.8	1.8	0.2	0	0
SRTM	0.0833	40.4	19.8	3.4	0.2	0
	0.417	29.2	0.6	0	0	0
	0.833	26.0	0.2	0	0	0

NLS, nonlinear least square; SRTM, simplified reference tissue model.

of Risperidone 0.5 mg were 0.866 and 0.496, then its occupancy resulted in 42.7%.

Scan duration: On the basis of the bootstrap approach, the relationship between the reliability of BP_{ND} and occupancy estimates and the scan duration was investigated as shown in Figure 5.

As scanning time became shorter, BP_{ND} in both before and after antipsychotics administration for two volunteers was overestimated. However, the bias of occupancy was small despite short scan durations. The COVs of both BP_{ND} and occupancy also became larger with shorter scan durations. These observations are consistent with the simulation results especially in the case of occupancy shown in Figure 3B, even though a small difference of magnitude of bias in BP_{ND} was still observed.

Discussion

In this study, we evaluated the effect of noise and scan duration of dynamic PET [^{11}C]MNPA studies on the BP_{ND} estimates obtained with NLS and SRTM for a range of BP_{ND} values, a range that is likely to be encountered in occupancy studies with antipsychotic medication. Error analysis was performed using artificial datasets. The validity of the simulations was assessed by using the bootstrap on a small cohort of human data to calculate 'real variances' that resulted in good agreement with those obtained from the artificial datasets.

Reliability of estimated parameters

In the case of NLS, the larger number of parameters introduced instability and, even though we introduced a fixed K_1/k_2 ratio, the variability of BP_{ND} was still significant as shown by the percentage of outliers by NLS (Table 2). K_1/k_2 for both target and reference regions were same in this simulation study; however, in clinical situation, sometimes K_1/k_2 values may vary from regions to regions (Ginovart *et al*, 2007) and these difference may introduce errors in BP_{ND} when the ratio K_1/k_2 is fixed.

The SRTM provided reliable estimates although variability increased for low BP_{ND} values even with favorable noise levels (Gunn *et al*, 1997; Ikoma *et al*, 2008). As shown in Figure 2B, both bias and COV with small $BP_{ND} = 0.0833$ were larger than those with $BP_{ND} = 0.417$ or 0.833. The small bias of BP_{ND} estimates in noise-free TACs (Figure 2B) may originate from the two-tissue model of the target

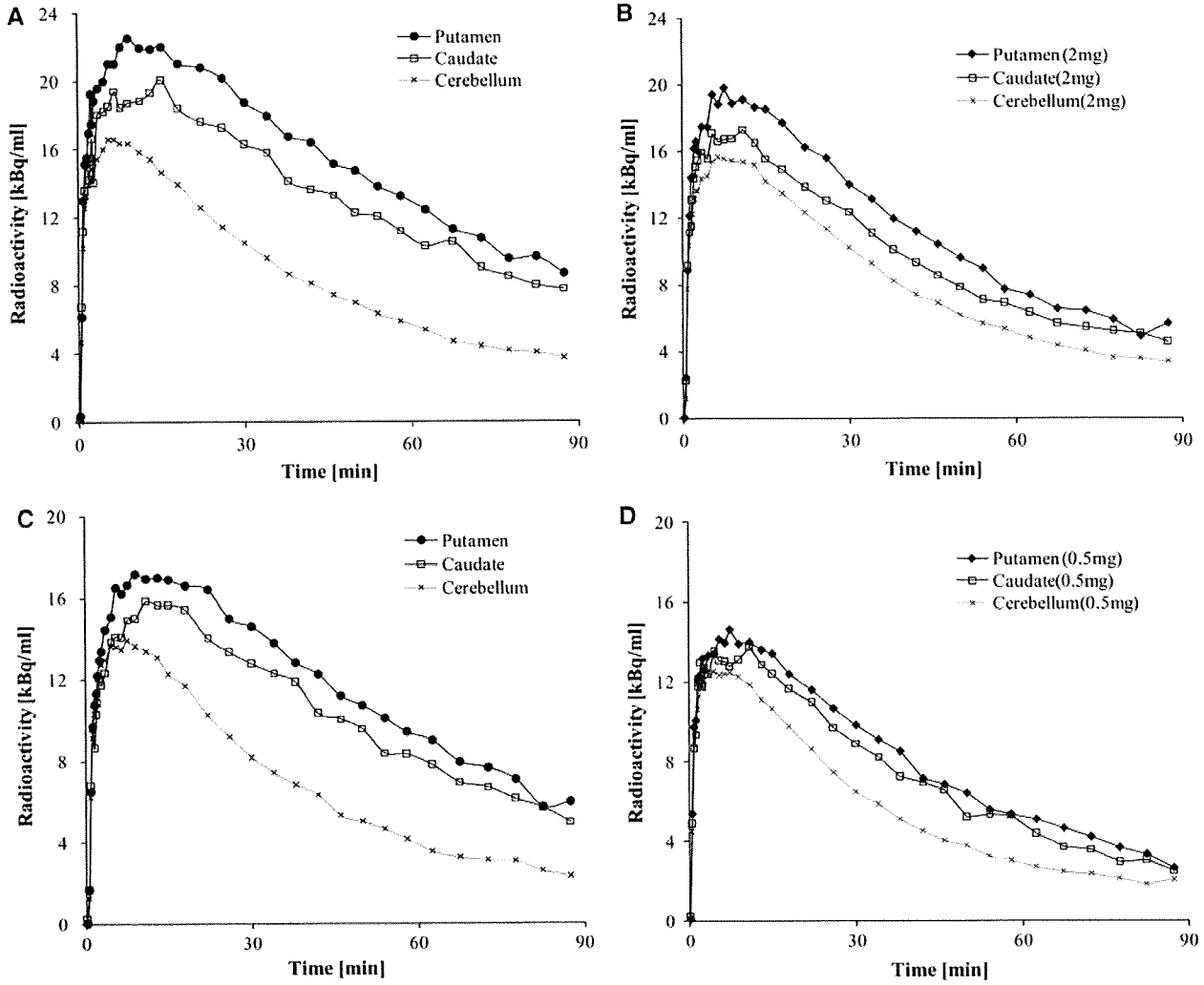

Figure 4 TACs for a single subject with baseline (**A**), and 2 mg administration of Risperidone (**B**), TAC for the other subject with baseline (**C**), and 0.5 mg administration of Risperidone (**D**). ROIs were drawn on putamen, caudate, and cerebellum.

tissue. In the SRTM method, even when the one-tissue model for target tissue is not appropriate, the apparent rate constant ($=k_2/(1+BP_{ND})$ in Equation (3) could be used to fit the curves well and bias in BP_{ND} is negligible (Wu and Carson, 2002). In this study, as shown in Figure 2B, the bias of BP_{ND} was small and the error propagation of biased BP_{ND} to occupancy in the SRTM method was also small. Errors of both estimated BP_{ND} and occupancy by SRTM were small at a low noise level, indicating that ROI analysis of SRTM will be useful for a quantified BP_{ND} and occupancy study with [^{11}C]MNPA.

In the simulation study, the reference TAC was assumed as noise free; however, noise may affect the reference TAC depending on the size of ROI (Ogden and Tarpey, 2006). For SRTM, the use of a 1% noise on the reference TAC increased %COV of the BP_{ND} estimates for the target regions (where noise was 3%) by 20% to 30%. However, the noise in the reference TAC did not change the profile of BP_{ND} %COV in the target TAC according to scan duration nor changed the biases in the estimated occupancies that remained similar.

Effects of scan duration

In the simulation study, a 60-min scan duration gave unbiased and reliable BP_{ND} and occupancy estimates by NLS with [^{11}C]MNPA both at baseline and with drug load (Figure 3A). Conversely, the results of SRTM method showed that at least 60-min scan duration would be required for the quantification of occupancy; bias was under 3% at a 3% noise level with scan duration longer than 60 mins (Figure 3B). Shorter scan duration caused larger bias of BP_{ND} estimated by SRTM. Note that the sampling rate of the reference input function is inherently lower than

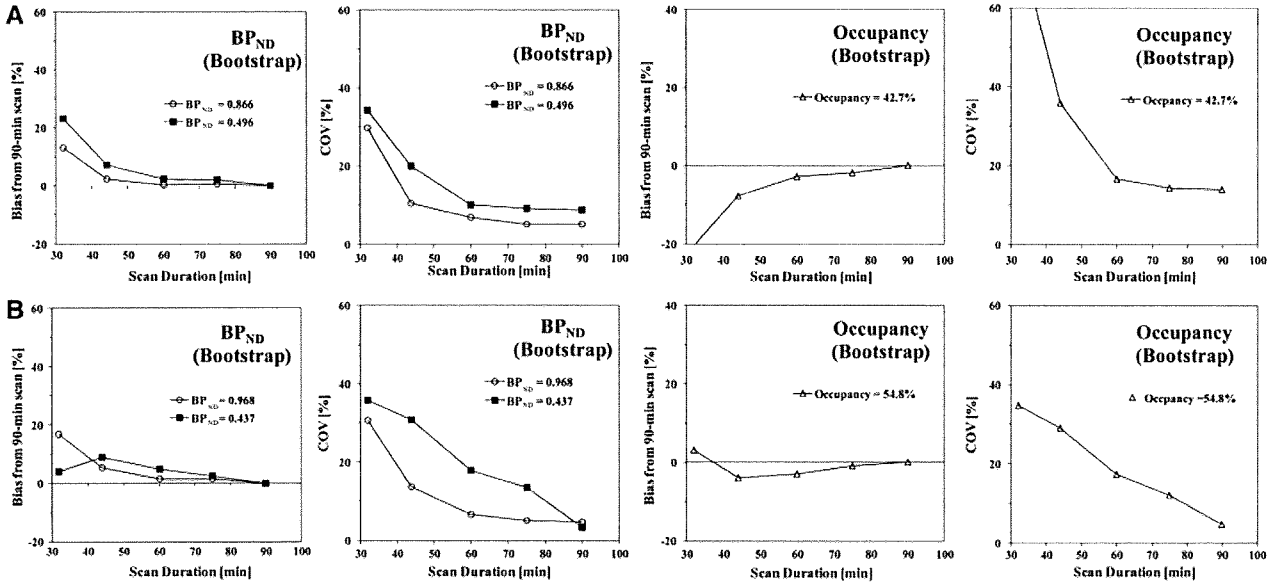

Figure 5 Scan duration dependency of bias and COV of BP_{ND} and occupancy in the putamen estimated by SRTM method for a single subject with 0.5 mg administration (**A**) and the other subject with 2 mg administration (**B**).

the one of the plasma input function and this may introduce errors with SRTM although in this instance, kinetics in tissue are not particularly fast.

The use of the bootstrap approach on clinical data validated most of the observations obtained from simulations for the SRTM method, such as the overestimation of BP_{ND} and underestimation of occupancy at shorter scan durations. It is important to remark that the variability considered here is the one associated with the measurement error only. Further variability of biological origin (between subjects and/or associated with age, gender, etc. (Inoue *et al*, 2001; Kaasinen *et al*, 2001)) should be taken into account and possibly controlled at the design stage.

We can therefore conclude that, for both NLS and SRTM methods, reliable and unbiased occupancy estimates of [^{11}C]MNPA could be obtained by 60 mins, with COV of 50% occupancy remaining at 11.0% and 10.1%, respectively (Figure 3). In the case of lower occupancy than 50%, COV at 60-min scan duration may be >11% but no bias should be expected.

Conclusion

The effects of bias, variance, and scan duration in PET quantitative analysis of dopamine D_2 receptor occupancy using [^{11}C]MNPA were evaluated in a simulation study and validated using a bootstrap approach on clinical data. The results suggest that a reference approach with SRTM applied to ROI data with a scan duration of at least 60-mins PET scan duration represent a valid bioassay for the task.

Acknowledgements

This study was supported in part by Grants-in-Aid for Young Scientists (B) (No. 19700395) and by a consignment expense for the Molecular Imaging Program on 'Research Base for PET Diagnosis' from the Ministry of Education, Culture, Sports, Science and Technology (MEXT), Japanese Government and by the Royal Society, International Project Grant no. JP0871550, UK. We thank Dr Hiroshi Watabe for his valuable advice.

Conflict of interest

The authors declare no conflict of interest.

References

Farde L, Wiesel FA, Halldin C, Sedvall G (1988) Central D2-dopamine receptor occupancy in schizophrenic patients treated with antipsychotic drugs. *Arch Gen Psychiatry* 45:71–6

Farde L, Wiesel FA, Stone-Elander S, Halldin C, Nordstrom AL, Hall H, Sedvall G (1990) D2 dopamine receptors in neuroleptic-naive schizophrenic patients. A positron emission tomography study with [11C]raclopride. *Arch Gen Psychiatry* 47:213–9

Ginovart N, Willeit M, Rusjan P, Graff A, Bloomfield PM, Houle S, Kapur S, Wilson AA (2007) Positron emission tomography quantification of [11C]-(+)-PHNO binding in the human brain. *J Cereb Blood Flow Metab* 27:857–71

Gunn RN, Lammertsma AA, Hume SP, Cunningham VJ (1997) Parametric imaging of ligand-receptor binding in PET using a simplified reference region model. *Neuroimage* 6:279–87